Microchim Acta (2016) 183:1375–1384
DOI 10.1007/s00604-016-1759-x

ORIGINAL PAPER

Immunoassay for troponin I using a glassy carbon electrode modified with a hybrid film consisting of graphene and multiwalled carbon nanotubes and decorated with platinum nanoparticles

Shobhita Singal[1,2] · **Avanish K Srivastava**[1] · **Bhasker Gahtori**[1] · **Rajesh**[1,2]

Received: 19 November 2015 / Accepted: 18 January 2016 / Published online: 10 February 2016

Abstract This article describes a bioelectrode for the determination of human cardiac troponin-I (cTnI). A glassy carbon electrode was coated with a hybrid film of graphene and multiwalled carbon nanotube (G-MWCNT) and modified with platinum nanoparticles (Pt NPs) that were capped with mercaptopropionic acid. The PtNPs were anchored on the G-MWCNT hybrid film via the cross-linker 1-pyrenemethylamine and subsequently functionalized with antibody against troponin (anti-cTnI). The bioelectrode was characterized by transmission electron microscopy, scanning electron microscopy, cyclic voltammetry, and electrochemical impedance spectroscopy. The performance of the immunoelectrode was investigated by electrochemical impedance spectroscopy, and response was fit to Randle's equivalent circuit model. The charge transfer resistance (R_{et}) at a.c. frequencies of <1 Hz is found to be a viable sensing parameter. The dissociation constant of the immunoreaction between surface immobilized anti-cTnI and the analyte cTnI is 0.29 nM (with a Hill coefficient of 0.23), this indicating a negative cooperativity and high binding affinity of cTnI for anti-cTnI on the electrode surface. The EIS response is linear in the 1.0 pg mL^{-1} to 10 ng mL^{-1} concentration range, and the R_{et} sensitivity is 145.5 Ω cm^2 per decade.

Keywords High resolution transmission electron microscopy · Cyclic voltammetry · Bioelectrode · Graphene · Electrochemical impedance spectroscopy · Biomarker · Myocardial infraction

Introduction

Composite materials of graphene and carbon nanotubes have been reported [1, 2] to establish synergistic effects between these two different graphitic nanostructures both having excellent electronic, thermal, optical and mechanical properties [3, 4]. Graphene, an allotrope of carbon, is a one-atom thick two dimensional layer of graphite with sp^2 bonded carbon atoms arranged in a hexagonal lattice [5]. Due to its unique physical properties such as high specific surface area, rapid heterogeneous electron transfer, great mechanical strength and relatively low manufacturing cost, graphene is an ideal material for the preparation of electrochemical biosensors [6, 7]. However, the outstanding properties of graphene emerge only in the planar direction. On the other hand, carbon nanotubes, hollow cylinder of sp^2 bonded carbon atoms, orients conductivity path in the axial direction. Thus, a graphene-carbon nanotube (G-CNT) hybrid which combines the unique properties of the two carbon allotropes in all directions could be an ideal electrode material for biosensors. The integrated structure of G-CNT has the fundamental advantage of combining the high specific surface area and three-dimensional

Electronic supplementary material The online version of this article (doi:10.1007/s00604-016-1759-x) contains supplementary material, which is available to authorized users.

✉ Rajesh
rajesh_csir@yahoo.com

[1] CSIR-National Physical Laboratory, Dr. K.S. Krishnan Road, New Delhi -110012, India

[2] Academy of Scientific and Innovative research (AcSIR), CSIR-National Physical Laboratory, Dr. K.S. Krishnan Road, New Delhi -110012, India

framework of CNT with the high edge-density of graphene [8]. Recently, several efforts have been made to fabricate G-CNT hybrid films via self-assembly of homogeneously mixed solutions of reduced graphene oxide and CNTs using surface functionalization techniques, and electrophoretic deposition [9–11]. However, these hybrid films are consist of overlapped thick graphene aggregates and are ineffective in creating the covalent C-C bonding between graphene and CNTs in the hybrid structure that reduces the total surface area of the hybrid film. Moreover these methods are multi-steps and quite tedious. Instead, the direct growth of G-CNT hybrids using chemical vapour deposition (CVD) method is more attractive on accounts of providing the covalent C-C bonding between the graphene and the CNTs with a comparatively lesser defect density and ease of scaling to multi-step chemical routes. Along with carbon supports, noble metal nanoparticles (NPs) are potential candidates in the development of electrochemical biosensors due to their high specific surface area, biocompatibility, excellent conductivity and chemical stability [12]. These materials have an additional advantage of enhanced diffusion due to convergent rather than linear diffusion at slow scan rates [13]. Many efforts have been devoted to synthesize noble metal NPs with uniform size and good dispersion over the carbon supports [14, 15]. Recently Li et al. synthesized a Pt/graphene composite using ethylene glycol as a reducing agent to directly reduce hexachloroplatinic acid (IV) acid and graphite oxide [16]. Pt NP directly loaded on carbon nanostructure has limited density and stability because of chemical inertness and atomic smooth surface of graphene. To obtain high-density and highly dispersed Pt-loaded G-MWCNT composite, we used 1-pyrenemethylamine as the interlinker, which can form a self-assembled layer on the surface of G-MWCNT via π-stacking interaction between the pyrene group and the graphene substrate [17]. The purpose of using carboxyl capped Pt nanoparticles is to provide site-specific protein immobilization of anti-cTnI with high loading and better probe orientation over the nanostructure surface of G-MWCNT for high binding affinity towards the target cTnI.

Cardiac troponin I (cTnI), a protein subunit of cardiac troponin complex, is an important biological index for the diagnosis of acute myocardial infarction (AMI). It binds to actin in thin myosin filaments to support the troponin-tropomyosin complex. cTnI is only restricted inside the myocardium and it is currently considered to be the standard biomarker test for detecting AMI, because it is significantly more specific than other cardiac biomarkers [18]. The levels of cTnI in healthy humans are normally lower than 0.1 ng mL^{-1}, and a level between 0.1and 2 ng mL^{-1} indicates a diagnosis of unstable angina and other heart disorder, whereas levels greater than 2 ng mL^{-1} indicate an increased risk for future serious heart events [19]. This emphasizes the need for developing diagnostic tools which are highly sensitive, cost effective, and utilizing existing large-scale manufacturing techniques. Conventional laboratory methods used for the quantitative detection of cTnI include enzyme-linked immunosorbent assay (ELISA) [20], chemiluminescence [21] and radioimmunoassay [22]. However, these methods suffer from numerous disadvantages such as long reaction time, multistep processing of samples, expensive reagents, and requirement for trained personnel. Electrochemical impedance spectroscopy (EIS) based immunosensing methods have attracted significant attention in recent years because of their rapidity, simplicity, high sensitivity, and non-destructive nature [23]. Recently, EIS based immunosensors have reported for the label-free ultrasensitive detection of cTnI and lipoprotein receptor-1 [24, 25].

We report on the fabrication of Pt NPs modified three-dimensional G-MWCNT hybrid film deposited on a glassy carbon electrode (GCE), as an impedimetric immunosensor, for ultrasensitive detection of cTnI in human serum. G-MWCNT hybrid was grown by chemical vapour deposition (CVD) method on a copper foil (25 μm thickness) deposited with ~1 nm thick Fe film and transferred on to a glassy carbon electrode (GCE), followed by surface modification with mercaptopropionic acid capped (MPA) capped PtNP using interlinker 1-pyrenemethylamine (PMA). The protein antibody, anti-cTnI, was covalently immobilized to pendant carboxyl groups of Pt(MPA) through carbodiimide coupling reaction to obtain the anti-cTnI-PtNP/G-MWCNT/GCE bioelectrode. The bioelectrode showed an enhanced electrochemical performance due to the uniform distribution of electroactive PtNP with large surface to volume ratio, over the G-MWCNT hybrid film.

Experimental

Chemicals and reagents

Antibody troponin I (anti-cTnI; Cat 4 T21 MAb 19C7) and antigen, human cardiac troponin I (cTnI; Cat 8 T53) were obtained from Hytest (Turku, Finland), Mouse immunoglobulin-G (IgG) (Cat IGP3) was obtained from GENEI, Bangalore, India. 1- Pyrenemethylamine hydrochloride, N-(3-dimethylaminopropyl)-N′-ethyl carbodiimide hydrochloride (EDC), N-hydroxysuccinimide 98 % (NHS), hydrogen hexachloroplatinate hexahydrate ($H_2PtCl_6 \cdot 6H_2O$), and 3-mercaptopropionic acid (MPA) were obtained from Sigma-Aldrich Corp. All other chemicals were of analytical grade and used without further purification.

Apparatus

TEM images were obtained on high resolution TM model Technai G2F30 STwin. SEM images were obtained on FE-SEM model SUPRA40 VP, Germany. Cyclic voltammetry

(CV) and EIS measurements were done on a PGSTAT302N, AUTOLAB instrument from Eco Chemie, The Netherlands. The EIS parameters were obtained by circuit fitting the EIS experimental data using GPES (General purpose electrochemical system version 4.9, Eco Chemie) software. All electrochemical measurements were carried out in a conventional three-electrode cell configuration consisting of a Pt-G-MWCNT based electrode/bioelectrode, as a working electrode, Ag/AgCl as reference electrode and platinum wire as counter electrode.

Synthesis of G-MWCNT hybrid

The G-MWCNT hybrid films were prepared with the slight modification of the previously reported procedure [26]. In brief, the G-MWCNT hybrid films were prepared by chemical vapour deposition technique on a copper foil deposited on its one side with ~1 nm thick Fe film using e-beam evaporator. The Fe deposited copper foils (1 × 1 cm^2) were placed in the fused silica tube (5 cm in diameter by 100 cm long) and were preheated at a temperature of 750 °C, under flowing Ar/H_2, 200 sccm (standard cubic centimetre per minute)/100 sccm atmosphere, for a period of 10 min, followed by injecting 10 sccm flow of acetylene (as a carbon source) for 20 min. At this temperature Fe film gets dewetted to form the Fe- nanoparticles, resulting to a simultaneous growth of both MWCNTs on Fe NPs and a graphene floor on residual Cu surface, respectively. The temperature of the furnace was cooled down to room temperature in flowing Ar/H_2 atmosphere to obtain the 3-dimetional nanostructure hybrid. Graphene film formed on the backside of the copper foil was removed by oxygen plasma (80 W, 30 min), followed by Cu etching in 1 M aqueous $FeCl_3$ solution to collect the G-MWCNT hybrid.

Preparation of the bioelectrode

Prior to modification, the glassy carbon electrodes (GCE, 3 mm in diameter) were polished with 1, 0.3 and 0.05 μm alumina powder successively, followed by sonication in distilled water and dried under vacuum. The G-MWCNT hybrid film was transferred on GCE surface (3 mm diameter) by careful scooping and dried at 50° C for 1 h to obtain the G-MWCNT/GCE. The G-MWCNT modified GCE so obtained were anodized at 1.7 V vs. Ag/AgCl for 500 s in pH 7.4 PB (0.1 M phosphate buffer), followed by cathodization at −0.6 V for 60 s to obtain an electroactive G-MWCNT. This treatment to G-MWCNT introduced defects on the edge planes of graphene surface and ends of carbon nanotubes with the generation of carbonyl groups during oxidation that were subsequently reduced to C-OH, leading to an enhanced electron transfer rate at the G-MWCNT, as reported earlier for GCE [27]. After this, G-MWCNT was functionalized with a molecular bilinker, PMA, through π- stacking, for the covalent attachment of Pt(MPA) nanoparticles. Pt (MPA) nanoparticles were chemically synthesized with a method as reported earlier [28]. G-MWCNT/GCE was incubated with 2 mM PMA in DMF for 40 min, at room temperature, followed by extensive washing with DMF and dried under N_2 gas flow to obtain the PMA functionalized G-MWCNT/GCE. The carboxyl groups of Pt (MPA) nanoparticles were activated into the corresponding esters by EDC/NHS treatment for partial covalent coupling on one hand with active amino group of PMA on G-MWCNT/GCE and the remaining on the other hand with active amino group of the anti-cTnI molecules for covalent biomolecular immobilization. 2.0 mL of 0.1 mg mL^{-1} aqueous solution of Pt (MPA) nanoparticles containing 0.15 M EDC and 0.03 M NHS was prepared and 10 μL of the above solution was drop casted on the PMA/G-MWCNT/GCE and left for 1 h, followed by washing with double distilled water to obtain the Pt(MPA)/G-MWCNT/GCE. The PtNP/G-MWCNT/GCE was biofunctionalized with anti-cTnI by incubating it with 10 μL PB containing 100 μg mL^{-1} anti-cTnI, at 4 °C for 2 h, followed by washing with PB and dried under N_2 gas flow. The bioelectrode was then incubated in 0.1 % bovine serum albumin (BSA) (*w*/*v*) to block the non-specific binding sites on the Pt(MPA) and the substrate surface as well, followed by washing with PB to remove the loosely bound antibody and dried under N_2 gas flow to obtain the desired anti-cTnI-PtNP/G-MWCNT/GCE bioelectrode. The stepwise fabrication of the bioelectrode is schematically represented in Fig. 1.

Result and discussion

Choice of materials

To develop a high-performance electrochemical immunosensor, the critical issues involved the immobilization of protein molecules with high loading and stability on the transducer matrix and efficient biomolecular electronic characteristics. Keeping this in view, we utilized a large surface area 3-dimentional hybrid of 2-dimentioanl graphene and 1-dimentional MWCNTs, as conducting matrix, where PtNPs are deposited for site specific immobilization of anti-cTnI for the construction of an impedimetric immunosensor. Graphene shows a better mechanical adhesion because of maximal contact area [29] whereas the CNT has high a surface to volume ratio. The synergetic combination of large surface area of MWCNT coupled with high conductivity and good adhesiveness of graphene with electroactive PtNP in the hybrid structure provides a better platform for site-specific biomolecular immobilization leading to high sensitive electrochemical detection of biomolecules. These characteristics makes nanocarbon materials a better choice as transducers than organic materials like conducting polymers, which are comparatively less stable in uneven environmental conditions

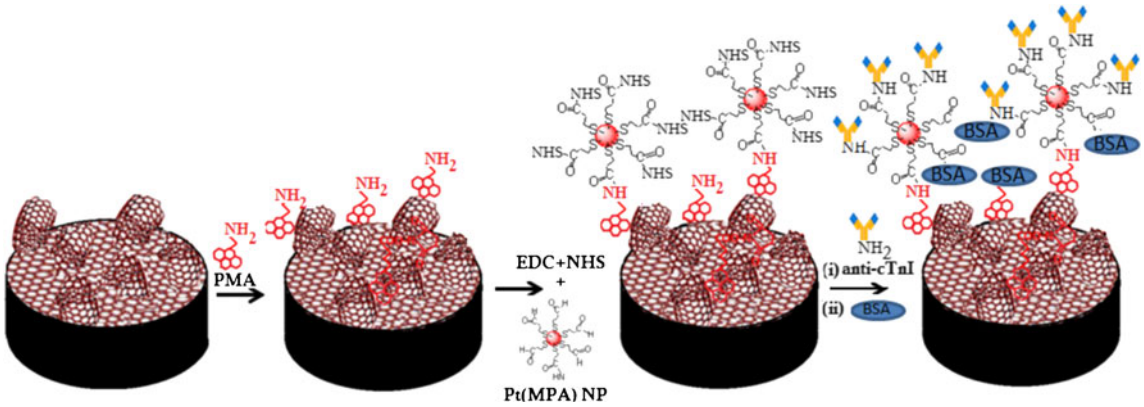

Fig. 1 Schematic representation of stepwise fabrication of the bioelectrode

of high temperature, pH, humidity, and electrochemical potential. Though both Au and Pt are excellent bioconjugates, the previous studies indicated that the electroactivity of Pt NP is a bit larger than that of Au NP [30]. Thus, we have chosen Pt NP as electroactive bioconjugate on G-MWCNT hybrid for the fabrication of an electroactive stable prototype for electrochemical sensing of cTnI.

Surface morphological characterization of the prepared Pt-G-MWCNT nanocomposite

High resolution transmission electron microscopy (HRTEM) was carried out on the samples of graphene embedded with multiwalled carbon nanotubes (MWCNTs) and platinum (Pt) nanoparticles (NPs). An ultrafine networking of carbon nanotubes was noted over graphene fine sheets throughout in the microstructure (Fig. 2a, b). Moreover a clear gray level contrast of Pt NPs was revealed on the networked MWCNTs in the graphene matrix (some of the Pt NPs are marked with a set of arrows in Fig. 2a, b). An atomic scale image of graphene nanosheet shows a hexagonal honeycomb-like structure of a typical graphene with fringe spacing of about 0.34 nm (inset I in Fig. 2a). Inset II in Fig. 2a elucidates that the Pt nanoparticles of facetted morphology range in size between 5 to 10 nm. Inset III in Fig. 2b further shows an ultrafine Pt nanoparticle trapped within the core diameter of a carbon nanotube. A corresponding selected area electron diffraction pattern (SAEDP) recorded on the composite of graphene dispersed with carbon nanotubes and platinum nanoparticles exhibited a set of few Debye rings (Fig. 2c). Although the two strong Debye rings evolved in reciprocal space due to the presence of first and second order diffraction planes of graphene, a few faint rings are attributed to the diffraction planes corresponding to 111 and 200 of the cubic crystal structure of Pt. The Pt rings in reciprocal space are quite diffuse, probably because of the ultrafine nature of the particles with multiple interfacing between graphene and carbon nanotubes. The SEM image of G- MWCNT hybrid shows uniform and highly dense distribution of MWCNT over the entire graphene surface (Please see Fig. S1 in the supporting information).

Electrochemical characterization of the bioelectrode

Cyclic voltammetry (CV) is convincing and widely used electroanalytical technique for investigation and monitoring the various stages of immunosensor fabrication. The alteration in peak current and separation of peak potentials in voltammograms at different electrode surfaces are theoretically related to the electron transfer rate constant i.e. the electron transfer resistance. Each step of surface modification of GCE was monitored by CV measurements carried out in a mixture of 2 mM $K_3[Fe(CN)_6]$ and 2 mM $K_4[Fe(CN)_6]$, as a redox probe,

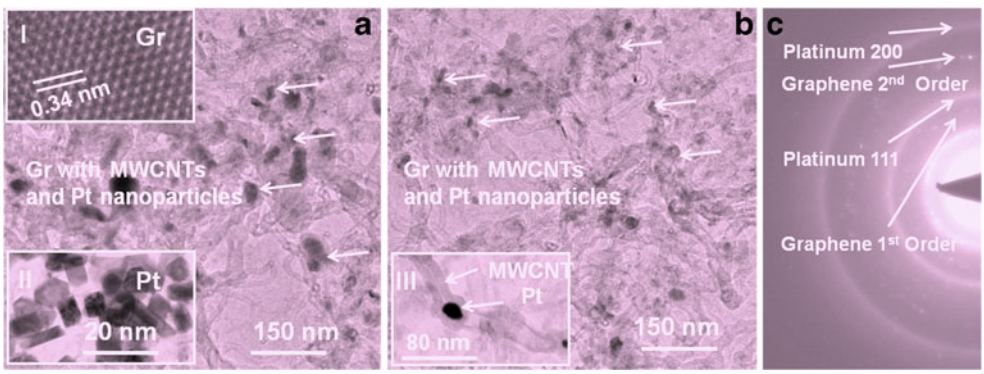

Fig. 2 HRTEM measurements showing **a**, **b** composite microstructure of Graphene with MWCNTs and Pt nanoparticles and **c** corresponding SAEDP. Insets: (I) atomic scale image of Graphene, (II) different size distribution of Pt nanoparticles, and (III) a single Pt particle in a carbon nanotube

in PB (pH 7.4, 0.1 M) containing 0.1 M KCl. The CV curves demonstrated that the voltammetric behaviour of redox probe $[Fe(CN)_6]^{3-/4-}$ was influenced by the electrode surface modification. The cyclic voltammogram of the modified electrode before and after the immobilization of a bioreceptor, anti-cTnI is shown in Fig.3. As can be seen, well-defined quasi-reversible redox cyclic voltammogram with anodic to cathodic current peak ratio of approximately one and peak-to-peak separation of 130 mV was observed for bare GCE. The electrochemical behaviour of the CVD grown G-MWCNT modified GCE after subjecting to simultaneous anodic and cathodic treatment exhibited a reversible CV with a comparatively small peak-to-peak potential separation (ΔE_p) of 59 mV and increased redox peak current with respect to bare GCE, indicated to an enhance heterogeneous electron transfer kinetics. The anodization of G-MWCNT produces oxygenated groups on its surface which contributed to an increased capacitive charging current. However, a decrease in redox peak current with increased ΔE_p of 104 mV was observed in PMA functionalized G-MWCNT/GCE. This may be due to the hydrophobic character of PMA that formed a physical barrier causing a decrease in the flux of redox probe to the electrode surface and thereby showing sluggish heterogeneous electron transfer kinetics, confirming the formation of PMA/G-MWCNT/GCE. A further decrease in CV peak current and increased ΔE_p of 208 mV was observed with the EDC/NHS activated Pt(MPA) NP modified G-MWCNT/GCE. This may be attributed to a repulsive interaction occurring in between the anionic redox probe and negatively charged terminal hydroxyl group of NHS [31]. Subsequent decreases in redox peak current were observed corresponding to the biomolecular immobilization of PtNP/G-MWCNT/GCE with anti-cTnI and its surface passivation with a blocking protein, BSA, respectively, due to insulating nature of the protein backbone chain structure [32].

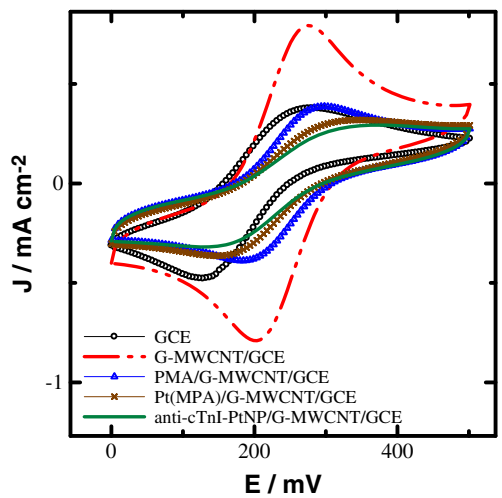

Fig. 3 CV of the bioelectrode at different stages of fabrication in PB (0.1 M KCl; pH 7.4) containing 2 mM $[Fe(CN)_6]^{3-/4-}$; scan rate 50 mV s^{-1}; 3rd CV scan is shown

The CV results were further elaborated by EIS, which was used to investigate the changes in impedance at the electrode solution interface in a wide frequency range (10,000 Hz to 0.01 Hz) of an applied perturbation of small amplitude AC voltage. The impedance result can be interpreted by fitting with modified Randles' equivalent circuit. In the modified circuit, the ohmic resistance of an electrolyte solution between the working electrode and the counter electrode is represented by R_s; C_{dl} is the double layer capacitance relating to the surface characteristics of the electrode; and R_{et} is the charge transfer resistance of the redox couple. The Warburg impedance (Z_w) with a semi-infinite diffusion mechanism in the measurement system arises from the diffusion resistance of the $[Fe(CN)_6]^{3-/4-}$ redox probe between the bulk solution and the interface of the modified working electrode. The EIS experimental data obtained during stepwise fabrication of the bioelectrode were fitted to the Randles equivalent circuit and the corresponding values of the EIS parameters are listed in Table 1. Taking into account the effect of the roughness of electrode surfaces, the constant phase element (CPE) is chosen to replace the ideal C_{dl} element. The impedance of a CPE is represented by Eq.1

$$Z_Q = \frac{1}{j\omega^n Y_\circ} \quad (1)$$

Where Y_o is a proportionality constant, ω is the angular frequency ($\omega = 2\Pi f$ in Hz), j is the imaginary number ($j = \sqrt{-1}$) and n ($-1 \le n \le 1$) corresponds to the heterogeneity of the electrode surface. CPE can represent capacitance($C = Y_o$) when $n = 1$; resistance ($R = 1/Y_o$) when $n = 0$; inductance ($L = 1/Y_o$) when $n = -1$ or Warburg impedance when $n = 0.5$. In our case, the value of n for distinct modified electrodes is <1, indicating a pseudo interfacial double layer capacitance at electrode/electrolyte interface. The chi-squared function (χ^2), which is the square of the standard deviation between the original data and the calculated spectrum, was found to be 0.016 for the bioelectrode, where the fitting lines nearly match Bode and Nyquist curves, indicating the best fit equivalent circuit.

The EIS Nyquist plot obtained at different stages of electrode fabrication is shown in Fig. 4. It was observed that the EIS of bare GCE displayed R_{et} of 70.8 Ω cm^2 with CPE parameter $Y_0 = 0.07$ mF cm^{-2} and $n = 0.81$. A significant fall in the R_{et} value to 0.30 Ω cm^2 with a corresponding increase in Y_0 to 0.28 mF cm^{-2} was observed with an almost straight line at all frequencies in the EIS for electroactive G-MWCNT/GCE. This may be ascribed to the fast electron exchange kinetics ($k^0 = 9.3 \times 10^{-2}$) and a diffusion limited process ($n = 0.46$) due to the large electroactive surface area of G-MWCNT hybrid film and edge plane defects, respectively. Thereafter, the PMA functionalization of G-MWCNT/GCE

Table 1 CV and EIS characteristics parameters at various stages of electrode surface modifications

Type of Electrodes	ΔE_p (mV)	R_{et} (Ωcm^2)	CPE		k^0 (m s^{-1})	Z_w (Ω cm^2)	χ^2 ($\times 10^{-2}$)	RSD (%) $n = 3$
			Y_0 ($\mu F cm^{-2}$)	n				
Bare GCE	128	70.8	70.1	0.81	3.8×10^{-4}	1.91×10^{-5}	1.28	12.2
G-MWCNT/GCE	59	0.3	283	0.46	9.3×10^{-2}	6.57×10^{-5}	7.84	9.2
PMA/G-MWCNT/GCE	104	44.8	15.2	0.88	6.0×10^{-4}	5.62×10^{-5}	2.99	23.3
PtNP /G-MWCNT /GCE	208	95.7	7.3	0.88	2.8×10^{-4}	4.76×10^{-5}	1.64	18.5
anti-cTnI-PtNP/G-MWCNT/GCE	324	669.9	30.5	0.85	4.0×10^{-5}	4.74×10^{-5}	3.04	19.5

ΔE_p = redox potential; R_{et} = charge transfer resistance; CPE = constant phase element; k^0 = apparent rate constant; Z_w = Warburg impedance

resulted into a sharp increase in R_{et} value to 44.8 Ω cm^2 due to the hydrophobic nature of PMA and a subsequent modification with EDC/NHS activated Pt(MPA) NP showed a further increase in the R_{et} value to 95.7 Ω cm^2 due to electron perturbation between the negatively changed NHS ester and anionic probe $[Fe(CN)_6]^{3-/4-}$ at the electrode surface.

The electrode surface coverage (θ) was calculated by using Eq. 2

$$\theta = 1 - \frac{R_{et1}}{R_{et2}} \quad (2)$$

Where θ represents the fraction of occupied binding sites; R_{et1} and R_{et2} represents the surface specific charge transfer resistance of PMA/G-MWCNT/GCE and PtNP/G-MWCNT/GCE, respectively. The value of θ was found to be 0.58, signifying ~58 % surface coverage of the electrode with Pt(MPA) nanoparticles. The site specific immobilization of antibody on EDC/NHS activated Pt(MPA) NP/G-MWCNT/GCE and the subsequent blocking of the non-specific binding sites by BSA showed a large increase in the the diameter of the semicircle (inset of the Fig. 4) with a R_{et} of 669.9 Ω cm^2 due to the severe inhibition of probe transfer by the large protein backbone chain, confirming the formation of the bioelectrode.

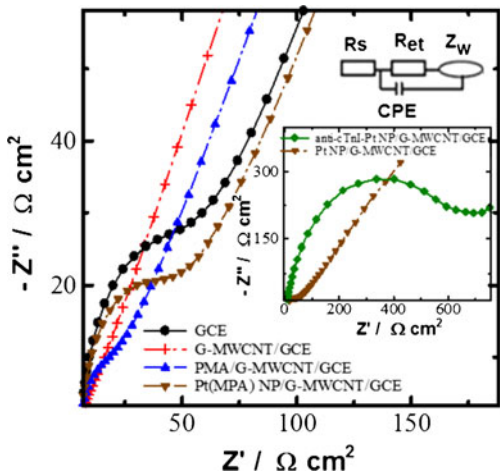

Fig. 4 Nyquist plot obtained at different stages of the bioelectrode fabrication in PB (0.1 M KCl; pH 7.4) containing 2 mM $[Fe(CN)_6]^{3-/4-}$

Electrochemical detection of cTnI

EIS response studies of the bioelectrode were carried out towards the protein antigen, cTnI, spiked in normal human serum. EIS measurements were taken each time after incubating the bioelectrode with individual 10 μL spiked human serum sample of different cTnI concentration for 10 min, followed by washing with PB and dried under N_2 gas flow, at room temperature. Since no significant change in EIS measurement was observed after 10 min of sample incubation of the bioelectrode, it was taken as an optimum incubation time for the completion of immunoreaction. Figure 5 shows the Nyquist and the corresponding Bode plot of the bioelectrode on immunoreaction with different concentration of cTnI spiked human serum. Since, major changes were observed in R_{et} amongst the various circuit elements, it was taken as a suitable sensing element for monitoring the immunoreaction towards the cTnI. The sample solution with a non-spiked human serum (without cTnI) was taken as the control sample and the corresponding R_{et} value was taken as the control sample response. The diameter of the semicircle in the Nyquist plot (Fig 5a) increased gradually upon incubation of the bioelectrode with increasing concentration of the cTnI spiked human serum due to antibody- antigen-complex formation upon immunoreaction, which acts as a kinetic barrier to interfacial electron transfer at the bioelectrode/solution interface. This results to an increasing R_{et} with decreasing capacitance (Y_0) values (Table 2) in the EIS response. These results were further elaborated by the corresponding Bode plot (Fig. 5b). In the Bode plot, at $f > 100$ Hz the impedance was independent of frequency with a nearly zero phase angle (Φ) and this corresponds to a solution resistance, R_s. In the intermediate frequency region of 1 to 100 Hz, the Bode plot showed the slope of −0.3 for log lZl vs log f with $\Phi < 90^\circ$ indicated to a pseudo- capacitive behaviour of the bioelectrode, since the slope of < -1.0 or Φ is $\geq 90^\circ$ corresponds to an ideal capacitive behaviour [33]. At $f < 0.1$ Hz, where current-time (I/t) vs. voltage-time (V/t) were found to be nearly in phase (lowest phase angle) with different cTnI concentration showed a dominant R_{et} characteristic, and confirmed our choice of using changes in R_{et} as the main sensing element.

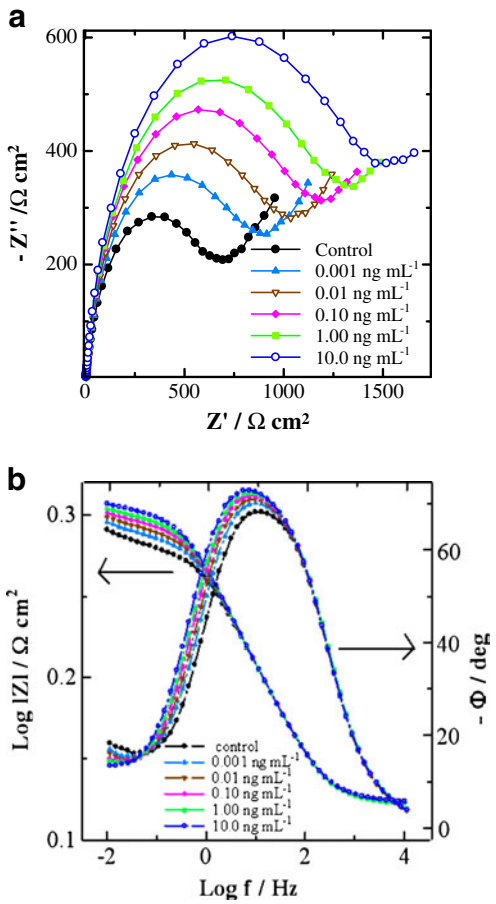

Fig. 5 **a** Nyquist plot of the bioelectrode before and after incubation with different concentration of cTnI-spiked human serum in PB (0.1 M KCl; pH 7.4) containing 2 mM $[Fe(CN)_6]^{3-/4-}$; **b** corresponding Bode plot

The dissociation constant is an important measurement in biological assays as a parameter to assess the affinity of interactions. The equilibrium dissociation constant (K_d) was measured to estimate the binding affinity of antigen to antibody in a bimolecular interaction using a Hill equation. The lower the K_d value (low concentration) higher is the binding affinity of the antigen to the antibody. The detailed binding equations of dissociation constant of antigen-antibody complex are given in supporting information. The value of K_d and Hill coefficient (n) was calculated from the ordinate intercept and slope of the Hill plot (Fig. 6a), respectively. The K_d was found to be 8.57 ng mL^{-1}, which corresponds to 0.29 nM. This low value of K_d indicated a strong binding affinity of cTnI towards anti-cTnI at the electrode surface, as any value less than micromolar concentration is considered to be quite good for a strong antigen-antibody interaction [34]. The Hill coefficient 'n', describes the cooperativity of antigen binding. If $n > 1$, the cooperativity is positive, when the antigen molecule binds to the specific antibody, the affinity of the antibody to other antigens increases. If $n < 1$, the cooperativity is negative i.e. the antigen molecule binds to the specific antibody and the affinity of the antibody to other antigens decreases. If $n = 1$, no cooperativity is observed and each binding site functions independently [35]. The n = 0.23 found in the present case corresponds to a negative cooperativity, which indicates the binding of cTnI to more than one anti-cTnI at the bioelectrode surface [36]. This may be due to the inhibition of multiple cTnI molecules binding to small aggregates or clusters of anti-cTnI due to steric hindrance [37].

Fig.6b shows the calibration curve of the bioelectrode representing a linear relationship between the change in charge transfer resistance ($\Delta R_{et} = (R_{et})_{\text{after immunoreaction}} - (R_{et})_{\text{control}}$) and the cTnI concentration over the range of 1.0 pg mL^{-1} to 10 ng mL^{-1} and can be represented by Eq. 3

$$\Delta R_{et}(cTnI) = b[cTnI] + 574.96 \quad (3)$$

The sensitivity of the bioelectrode (slope of the calibration curve) was found to be 145.5 Ω cm^2 per decade with a correlation coefficient of 0.99. This sensitivity of the bioelectrode is significantly high, which is about 1.8 time more than the recently reported sensitivity of the PtNP modified graphene based bioelectrode for cTnI detection [38] over a wide linear detection range of cTnI. This signifies the importance of the 3-Dimentional G-MWCNT over the 2D pristine graphene matrix with respect to a large electroactive surface area, which provided a comparatively large amount of PtNP deposition for site specific protein immobilization with a better probe orientation, showing a much wider linear detection range for cTnI than the earlier reported bioelectrodes [21, 25, 39–43] (Table 3).

Table 2 EIS characteristic parameters of the bioelectrode on immunoreaction with different concentration of target cTnI

Immunoreaction with [cTnI]	R_{et} (Ω cm^2)	CPE		Zw (Ω cm^2)	χ^2 (10^{-2})	RSD (%)
		Y_0 (μF cm^{-2})	n		(n = 3)	
Control	669.9	30.59	0.850	4.74×10^{-5}	3.04	-
0.001 ng mL^{-1}	847.7	29.62	0.857	4.61×10^{-5}	3.47	19.3
0.010 ng mL^{-1}	980.3	29.01	0.860	4.59×10^{-5}	3.68	13.2
0.10 ng mL^{-1}	1121.4	28.67	0.862	4.66×10^{-5}	4.57	8.5
1.00 ng mL^{-1}	1246.9	28.39	0.864	4.63×10^{-5}	4.58	1.20
10.0 ng mL^{-1}	1428.6	28.01	0.866	4.66×10^{-5}	4.72	4.03

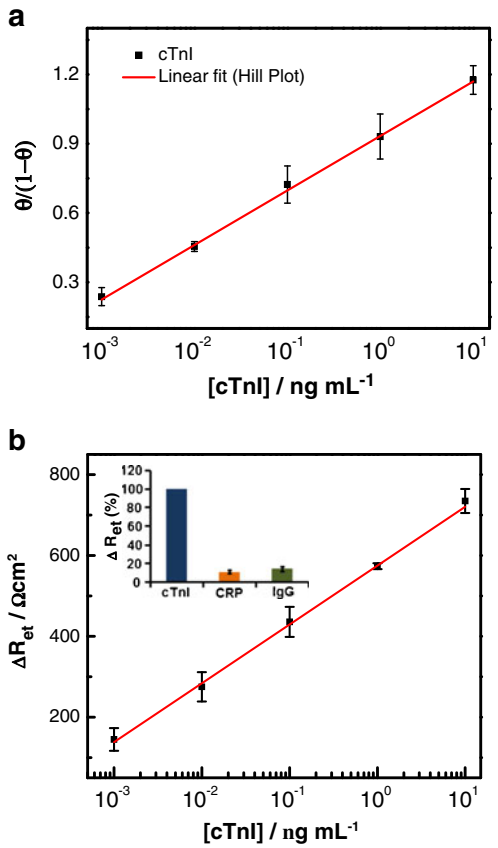

Fig. 6 **a** Hill plot for determining the dissociation constant (K_d) between the cTnI and anti-cTnI; **b** Concentration dependent calibration curve of the bioelectrode; inset: normalized response ΔR_{et} (%) of the bioelectrode towards non-specific CRP and IgG with respect to cTnI. The error bars represent the standard deviation from three separate experiments

Reproducibility, specificity and stability of the assay

The reproducibility of the bioelectrode was investigated in terms of relative standard deviation (RSD) by taking measurements with three different bioelectrodes prepared in the same manner and was found to be ±4 % for a maximum cTnI concentration of 10 ng mL^{-1}, suggesting a good reproducibility in the tested condition. The specificity of the bioelectrode was investigated by evaluating the normalized resistance response ΔR (%) upon exposure to each 10 ng mL^{-1} concentration of non-specific IgG and another cardiac biomarker, C-reactive protein (CRP), under identical conditions, as described for the specific target cTnI. It was observed that both the IgG and CRP showed normalized resistance response ΔR (%) of 14.6 % and 11.3 %, respectively, with respect to cTnI (inset of Fig 6b). These small changes in the resistance response towards the non-specific proteins indicate a good specificity of the bioelectrode for cTnI detection. The stability of the bioelectrode was also investigated by carrying out repeated EIS measurements with 1.0 ng mL^{-1} cTnI in human serum, under identical conditions. With an observation of getting almost consistent R_{et} response for more than six EIS measurements on the same sample of cTnI spiked human serum, it may concluded that the bioelectrode has a good stability in solution. However, the EIS responses decreases significantly after its storage of more than one month at room temperature and have therefore limited stability in an open environment.

Conclusion

In summary, we have demonstrated the impedance sensing performance of the bio-functionalized PtNP modified 3-dimentional carbon nanostructure of MWCNT and graphene deposited on GCE for cTnI. This Pt/G-MWCNT platform combine the advantages of porous and large surface area of the G-MWCNT with ultra-high density of active graphene edge planes together with high surface to volume ratio of electroactive Pt NP that allows an efficient covalent biomolecular immobilization, responsible for high protein loading and fast interfacial electron exchange. The bioelectrode exhibited a linear response over a wide concentration range of 1.0 pg mL^{-1} to 10 ng mL^{-1} cTnI-spiked human serum with high sensitivity of 145.5 Ω cm^2 per decade. This high sensitivity of the bioelectrode due to the high binding affinity of cTnI at the electrode surface, as depicted by Hill coefficient (n) = 0.23 where individual cTnI molecule is binding with more than one anti-cTnI, indicated a good biocompatibility of the bioelectrode. These results indicate that the above

Table 3 Comparative analytical performance of the bioelectrode with existing electrochemical systems for cTnI detection

Sensing methods	Transducing matrix	Detection range	Detection limit	Ref.
Electrocheminunesence	Au NPs	0.10 ng mL^{-1} to 1 μg mL^{-1}	60.0 pg mL^{-1}	[21]
Impedimetric	VACNF	0.25 ng mL^{-1} to 1 ng mL^{-1}	0.2 ng mL^{-1}	[25]
Amperometry	PDMS/Au	0.20 ng mL^{-1} to 10 μg mL^{-1}	148 pg mL^{-1}	[39]
Capacitive	Au/SPE	0.20 ng mL^{-1} to 12.5 ng mL^{-1}	0.2 ng mL^{-1}	[40]
Potentiometry	Au/ITO	1.0 ng mL^{-1} to 100 ng mL^{-1}	-	[41]
Stripping voltammetry	Ag/SPE	0.1 ng mL^{-1} to 32 ng mL^{-1}	0.1 ng mL^{-1}	[42]
Square-wave voltammetry	Ferrocene/Silica NP	-	24 pg mL^{-1}	[43]
Impedimetric	Pt/G-MWCNT	1.0 pg mL^{-1} to 10 ng mL^{-1}	1.0 pg mL^{-1}	Present method

mentioned Pt/G-MWCNT nanocomposite modified electrode may be used to immobilize other enzymes, proteins or DNA for various biological and electrochemical applications. Besides having the advantage of low cost and simple analytical method discussed above, the present system has the disadvantage of having a limited stability at room temperature in an open environment.

Acknowledgments We are grateful to Director, National Physical Laboratory, New Delhi, India for providing research facilities. Shobhita Singal is thankful to CSIR for providing a senior research fellowship. We are also thankful to Mr. V.K. Tanwar and Mr. Vikash Sharma, for technical help.

Compliance with Ethical Standards The author(s) declare that they have no competing interests

References

1. Stankovich S, Dikin DA, Dommett GHB, Kohlhaas KM, Zimney EJ, Stach EA, Piner RD, Nguyen ST, Ruoff RS (2006) Graphene-based composite materials. Nature 442:282–286
2. Coleman J, Khan U, Gunko Y (2006) Mechanical reinforcement of polymers using carbon nanotubes. Adv Mater 18:689–706
3. Geim AK (2009) Graphene: status and prospects. Science 324: 1530–1534
4. Popov VN (2004) Carbon nanotubes: properties and application. Mater Sci Eng 43(3):61–102
5. Novoselov KS, Geim AK, Morozov SV, Jiang D, Zhang Y, Dubonos SV, Grigorieva IV, Firsov AA (2004) Electric field effect in atomically thin carbon films. Science 306: 666–669.
6. Fowler JD, Allen MJ, Tung VC, Yang Y, Kaner RB, Weiller BH (2009) Practical chemical sensors from chemically derived graphene. ACS Nano 3:301–306
7. Pumera M, Ambrosi A, Bonanni A, Chng ELK, Poh HL (2010) Graphene for electrochemical sensing and biosensing. Trends Anal Chem 29:954–965
8. Henry PA, Raut AS, Ubnoske SM, Parker CB, Glass JT (2014) Enhanced electron transfer kinetics through hybrid graphene-carbon nanotubes films. Electrochem Commun 48: 103–106.
9. Jia F, Duan N, Wu S, Dai R, Wang Z, Li X (2015) Impedimetric salmonella aptasensor using a glassy carbon electrode modified with an electrodeposited composite consisting of reduced graphene oxide and carbon nanotubes. Microchim Acta doi:10.1007/s00604-015-1649-7.
10. Li S, Yan Y, Zhong L, Liu P, Sang Y, Cheng W, Ding S (2015) Electrochemical sandwich immunoassay for the peptide hormone prolactin using an electrode modified with graphene, single walled carbon nanotubes and antibody-coated gold nanoparticles. Microchim Acta 182:1917–1924
11. Zhu G, Yi Y, Zou B, Liu Z, Sun J, Wu X (2015) A glassy carbon electrode modified with a multiwalled carbon nanotube@reduced graphene oxide nanoribbon core-shell structure for electrochemical sensing of p-dihydroxybenzene. Microchim Acta 182:871–877
12. Teow Y, Valiyaveettil S (2010) Active targeting of cancer cells using folic acid-conjugated platinum nanoparticles. Nanoscale 2: 2607–2613
13. Jones SEW, Compton RG (2008) Fabrication and applications of nanoparticle modified electrodes in stripping analysis. Curr Anal Chem 4:177–182
14. Tang J, Tang D (2015) Non-enzymatic electrochemical immunoassay using noble metal nanoparticles: a review. Microchim Acta 182: 2077–2089
15. Zhang L, Wang J, Tian Y (2014) Electrochemical in-vivo sensors using nanomaterials made from carbon species, noble metals, or semiconductors. Microchim Acta 181: 1471–1484.
16. Li YJ, Gao W, Ci LJ, Wang CM, Ajayan PM (2010) Catalytic performance of Pt nanoparticles on reduced graphene oxide for methanol electro-oxidation. Carbon 48:1124–1130
17. Li W, Zhai D, Qiu H, Pang H, Pan L, Shi Y, Self-assembly synthesis of high density Pt nanoparticles on chemically reduced graphene sheets. Chem Lett. 40: 104–105.
18. Nusier MK, Ababneh BM (2006) Diagnostic efficiency of creatinine kinase (CK), CKMB, troponin T and troponin I in patients with suspected acute myocardial infarction. J Health Sci 52(2):180–185
19. Qureshi A, Gurbuz Y, Niazi JH (2012) Biosensors for cardiac biomarkers detection: a review. Sensors Actuators B 171-172: 62–76.
20. Wang J, Ibanez A, Chatrathi MP, Escarpa A (2001) Electrochemical enzyme immunoassays on microchip platforms. Anal Chem 73: 5323–5327
21. Li F, Yu Y, Cui H, Yang D, Bian Z (2013) Label free electrochemiluminescence immunosensor for cardiac troponin I using luminal functionalized gold nanoparticles as a sensing platform. Analyst 138:1844–1850
22. Apple FS, Falahati A, Paulsen PR, Miller EA, Sharkey S (1997) Improves detection of minor ischemic myocardial injury with measurement of serum cardiac troponin I. Clin Chem 43: 2047–2051.
23. Konsuphol P, Arya SK, Wong CC, Polla LJ, Park MK (2014) Coiled-coil peptide based sensor for ultra-sensitive thrombin detection. Biosens Bioelectron 55:26–31
24. Billah M, Hays HCW, Hodges CS, Ponnambalam S, Vohra R, Millner PA (2012) Mixed self-assembled monolayer (mSAM) based impedimetric immunosensors for cardiac troponin I (cTnI) and soluble lectin-like oxidized low-density lipopreotein receptor-1 (sLOX-1). Sensors Actuators B 173:361–366
25. Periyakaruppan A, Gandhiraman RP, Meyyappan M, Koehne JE (2013) Label-free detection of cardiac troponin-I using carbon nanofiber based nanoelectrode arrays. Anal Chem 85:3858–3863
26. Rajesh PRK, Mulchandani A (2013) Platinum nanoflowers decorated three-dimensional graphene-carbon nanotubes hybrid with enhanced electrocatalytic activity. J. Power Sources 223:23–29
27. Chou A, Bocking T, Singh NK, Gooding JJ (2005) Demonstration of the importance of oxygenated species at the end of carbon nanotubes on their favorable electrochemical properties. Chem Commun 7:842–844
28. Mishra SK, Srivastava AK, Kumar D, Rajesh (2014) Bio-functionalized Pt nanoparticles based electrochemical impedance immunosensor for human cardiac myoglobin. RSC Adv 4: 21267–21276
29. Biswas C, Lee YH (2011) Graphene versus carbon nanotubes in electronics devices. Adv Funct Mater 21: 3806–3826.
30. Bas SZ, Gulce H, Yildiz S, Gulce A (2011) Amperometric biosensors based on deposition of gold and platinum nanoparticles on polyvinylferrocene modified electrode for xanthine detection. Talanta 87:189–196
31. Sharma MK, Rao VK, Merwyn S, Agarwal GS, Upadhyay S, Vijayaraghavan R (2011) A novel piezoelectric immunosensor for the detection of malarial plasmodium falciparum histidine rich protein-2 antigen. Talanta 85:1812–1817
32. Pei R, Cheng Z, Wang E, Yang X (2001) Amplification of antigen-antibody interactions based on biotin labelled protein-streptavidin network complex using impedance spectroscopy. Biosens Bioelectron 16:355–361
33. Gomes EC, Oliveira MAS (2011) Corrosion protection by multilayer coating using layer-by-layer technique. Surf Coat Technol 205:2857–2864

34. Ohno Y, Maehashi K, Matsumoto K (2010) Label free biosensors based on aptamer-modified graphene field-effect transistors. J Am Chem Soc 132:18012–18013
35. Tajima N, Takai M, Ishihara K (2011) Significance of antibody orientation unravelled: well-oriented antibodies recorded high binding affinity. Anal Chem 83: 1969–1976.
36. Pathirana ST, Barbaree J, Chin BA, Hartell MG, Neely WC, Vodyanoy V (2000) Rapid and sensitive biosensor for salmonella. Biosens Bioelectron 15:135–141
37. Lerner MB, Souza JD, Pazina T, Dailey J, Goldsmith BR, Robinson MK, Jhonson CAT (2012) Hybrids of a genetically engineered antibody and a carbon nanotube transistor for detection of prostate cancer biomarkers. ACS Nano 6: 5143–5149.
38. Singal S, Srivastava AK, Biradar AM, Mulchandani A, Rajesh (2014) Pt nanoparticles chemical-vapor deposited graphene composite based immunosensor for the detection of human cardiac troponin I. Sensors Actuators B 205:363–370
39. Ko S, Kim B, Jo SS, Oh SY, Park JK (2007) Electrochemical detection of cardiac troponin I using a microchip with the surface-functionalized poly (dimethyl siloxane) channel. Biosens Bioelectron 23:51–59
40. Bhalla V, Carrara S, Sharma P, Nangia Y, Suri CR (2012) Gold nanoparticles mediated label-free capacitive detection of cardiac troponin-I. Sensors Actuators B 161:761–768
41. Ahammad AJS, Choi YH, Koh K, Kim JH, Lee JJ, Lee M (2011) Electrochemical detection of cardiac biomarker troponin-I at gold nanoparticle-modified ITO electrode by using open circuit potential. Int J Electrochem Sci 6:1906–1916
42. Shumkov AA, Suprun EV, Shatinina SZ, Lisitsa AV, Shumyantseva VV, Archakov AI (2013) Gold and silver nanoparticles for electrochemical detection of cardiac troponin-I based on stripping voltammetry. J Bionanosci 3:216–222
43. Jo H, Gu H, Jeon W, Youn H, Her J, Kim SK, Lee J, Shin JH, Ban C (2015) Electrochemical aptasensor of cardiac troponin I for the early diagnosis of acute myocardial infarction. Anal Chem 87(19): 9869–9875.